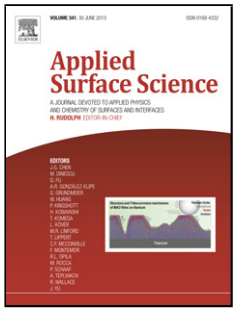

Title: Study on catalytic properties and carbon deposition of Ni-Cu/SBA-15 for cyclohexane dehydrogenation

Authors: Zhijun Xia, Huayan Liu, Hanfeng Lu, Zekai Zhang, Yinfei Chen

PII: S0169-4332(17)31291-6
DOI: http://dx.doi.org/doi:10.1016/j.apsusc.2017.04.245
Reference: APSUSC 35926

To appear in: *APSUSC*

Received date: 11-3-2017
Revised date: 27-4-2017
Accepted date: 29-4-2017

Please cite this article as: Zhijun Xia, Huayan Liu, Hanfeng Lu, Zekai Zhang, Yinfei Chen, Study on catalytic properties and carbon deposition of Ni-Cu/SBA-15 for cyclohexane dehydrogenation, Applied Surface Sciencehttp://dx.doi.org/10.1016/j.apsusc.2017.04.245

Study on catalytic properties and carbon deposition of Ni-Cu/SBA-15 for cyclohexane dehydrogenation

Zhijun Xia, Huayan Liu, Hanfeng Lu, Zekai Zhang, Yinfei Chen*

Institute of Catalytic Reaction Engineering, College of Chemical Engineering, Zhejiang University of Technology, Hangzhou 310014, PR China

*Corresponding author: Yinfei Chen, E-mail address: chfy@zjut.edu.cn, Tel: +86-13606643528.

Highlights:

- Bimetallic Ni-Cu NPs dispersed highly on SBA-15 were prepared by impregnation.
- The Cu addition into Ni suppresses the non-selective sites and coke formation.
- In-situ DRIFT study reveal the existence of alkenes in the reactive intermediates.
- The absorption of benzene on catalyst is stronger than that of cyclohexane.

Graphical Abstract

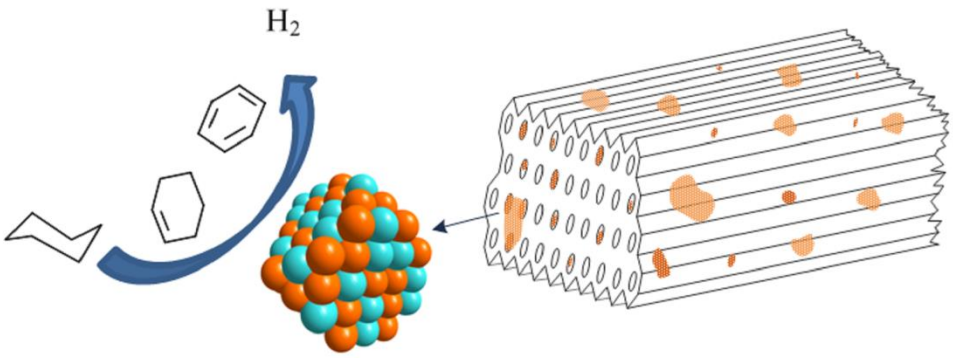

Abstract: A series of Ni-Cu supported on SBA-15 were prepared by impregnation, and used as catalysts in cyclohexane dehydrogenation for hydrogen production. The results indicated that the addition of Cu into Ni changes the crystal structure of metal Ni, and forms Ni-Cu alloy. Thus, Cu improves the reduction properties of Ni. Conversely, Ni stables and disperses metal Cu. With the space limitation of the ordered channels and high surface area of SBA-15, the bimetallic Ni-Cu/SBA-15 catalysts expose large amounts of selective active sites composed uniformly with Ni and Cu. Therefore, they present not only excellent catalytic performance for cyclohexane dehydrogenation, but also low coke formation. The in-situ

DRIFT studies have shown the vinyl species, indicating the existence of alkenes in the reactive intermediates. Additionally, the strong absorption of benzene on the metal could induce benzene was dehydrogenated further to carbon.

Keywords: Hydrogen storage; Dehydrogenation; Cyclohexane; Carbon deposition; Ni; Cu.

1. Introduction

As hydrogen storage and transport medium, liquid organic hydrocarbon is an attractive technology since they have high hydrogen storage density, and the hydrogenation process of dehydrogenated products is well developed in the industry [1-4]. Especially, the hydrogen in the dehydrogenation product is CO-free, and this is beneficial to proton exchange membrane (PEM) fuel cells which are highly sensitive to poisoning by CO [5-7]. Furthermore, cyclohexane which holds a high volumetric capacity of hydrogen about 56.0 g L^{-1} is provided with lower cost and much maturer technology than others. The catalysts and reactors for hydrogen production via dehydrogenation reaction of cyclohexane have been investigated in recent years [8-15].

Large studies indicated that Pt-based catalysts exhibited an excellent catalytic performance for cycloalkane dehydrogenation reaction [7,13-17]. However, the noble metallic catalysts have to increase the cost of hydrogen storage. Thus, some efforts for non-precious metal catalysts have been undertaken, such as Mo [18] or Ni [14,19-23]. In particular, Ni-based bimetallic catalysts presented the good activity of Ni and the high selectivity of the second metal (Ag, Sn, Zn [20], or Cu [14,21]).

In fact, the Ni or Ni-Cu catalysts had been studied for dehydrogenation of cyclohexane since the pioneer works by Sinfelt [24]. Pure Ni-based catalysts exhibit a high hydrogenolysis activity (C-C cleavage) [25]. With the addition of small amounts of Cu to Ni, much of the hydrogenolysis activity declined while the cyclohexane dehydrogenation activity (C-H cleavage) increased [24]. However, large amounts of selective active sites are required in order to product hydrogen effectively. Moreover, it is difficult to avoid the formation of un-selective sites, which are composed with monometallic Ni on the Ni-Cu catalysts prepared by conventional method. Thus, in order to highly dispersion and uniform bimetallic Ni-Cu

nanoparticles, the sol-gel technique was used in our previous paper [14]. Although the catalysts present good catalytic performance, mounts of active metal species could be covered by SiO_2 sol. In addition, due to the highly dispersion, the metallic particles are too small to be detected with surface characterization techniques. The catalytic properties and reaction mechanism of Ni-Cu for cyclohexane dehydrogenation are still not clearly.

Furthermore, the carbon deposition exists on the surface of metal Ni exposed to hydrocarbon, especially at high temperature [26,27]. To minimize coke formation over Ni-based catalysts, some methods by suppressing strong acidity of support have been attempted, such as modification of alkali metals [28,29] and application of neutral carrier SiO_2 [30,31]. Additionally, SBA-15 is a pure silica mesoporous molecular sieve, and has an advantage to grow and anchor metallic nanoparticles, due to its ordered structure, large surface area and pore volume [32-35]. Most of all, the dehydrogenation reaction at low temperature as possible is an effective strategy for inhibiting coke, by improving the catalytic performance of Ni-based catalysts.

In this work, SBA-15 has been applied to support the monometallic or bimetallic particles of Ni and Cu. In order to better understand the reactivity and explain the mechanism of catalytic reaction and coke formation, the catalysts were characterized by a variety of physic-chemical techniques.

2. Material and methods

2.1 Catalyst preparation

The Ni-Cu/SBA-15 catalysts were prepared via impregnation, using the similar procedure with that described in literature [35]. In briefly, the total 1.50 mmol of nitrate ($Ni(NO_3)_2 \cdot 6H_2O$ and $Cu(NO_3)_2 \cdot 3H_2O$, Sinopharm Chemical Reagent Co.) were dissolved in organic solvent mixed with 5.0 g alcohol (Sinopharm Chemical Reagent Co., 99.8% purity) and 5.0 g hexane (Sinopharm Chemical Reagent Co., 99.5% purity), and the mass loading of Ni to Cu has been listed in table 1. Then, 1.00 g SBA-15 zeolite (JCNANO, 685.4 $m^2\ g^{-1}$) was added to the impregnation solution. The mixture was dried for 24 h at room temperature and

24 h at 60 ℃. The solid product was calcined in air at 550 ℃ for 4 h. The calcined samples obtained were denoted as xNiyCu/SBA-15, where x and y were the mole ratio of Ni and Cu.

2.2 Materials characterization

The Brunaure-Emmett-Teller (BET) surface area and pore structure were obtained from nitrogen adsorption-desorption on a Micromeritics 3Flex Surface Characterization Analyzer. The powder X-ray diffraction (XRD) analysis was performed on a PANalytical X' pert PRO diffractometer with Cu Kα (λ = 0.154 nm). Transmission Electron Microscopy (TEM) study was performed on a Philips-FEI Tecnai G2 F30 S-Twin instrument. To characterize the chemical composition and metal elemental distribution on the surface of SBA-15, Scanning Transmission Electron Microscopy (STEM) coupled with Energy Dispersion X-ray Spectrum (EDS) was used. X-ray Photoelectron Spectroscopy (XPS) was on a Kratos AXIS Ultra DLD spectrometer with a monochromatic Al Kα 150 w X-ray source. Thermogravimetry (TG) analysis data was collected in a Netzsch STA409PC instrument. The samples were heated from 25 ℃ to 800 ℃ under 10% O_2 in N_2 (50 mL min^{-1}), and the heating rate was 10 ℃ min^{-1}.

Hydrogen-temperature-programmed reduction (H_2-TPR) experiments of samples were performed on a FineSORB-3010 apparatus. About 100 mg of the calcined sample was placed in a U-shape quartz reactor, and pretreated at 200 ℃ for 1.0 hour under Ar flow (30 mL min^{-1}). After cooling to 50 ℃, the gas flow was switched to 5% H_2 in Ar (30 mL min^{-1}). The sample was kept at 50 ℃ for 60 min, and then heated to 800 ℃ at 10 ℃ min^{-1}. The hydrogen consumption was recorded with a TC detector. In situ diffuse reflectance infrared Fourier transform (In-situ DRIFT) spectroscopy of the samples was detected on a Bruker Vertex70 apparatus using a reaction cell capped with KBr window. Signals were obtained from an MCT detector, and recorded 32 scans at resolution of 4 cm^{-1}. Firstly, the powder sample (catalysts or SBA-15) was placed in the reaction cell, and reduced at 450 ℃ for 4.0 hour in 5% H_2-95% Ar flow (30 mL min^{-1}). After cooling to 250 ℃, a reaction gas was switched and fed to the sample by bubbling cyclohexane through 0 ℃ buffer bottle with 5% H_2-95% Ar flow (30 mL min^{-1}).

2.3 Catalytic tests

The catalytic performance of catalysts for cyclohexane dehydrogenation was evaluated using a quartz U-shape fixed bed tubular 5 mm (Internal Diameter) reactor. Typically, 150 mg of the catalyst precursor (40-60 mesh) was placed into the center of the quartz reactor, with the each side of the sample packed with quartz wool. At first, the catalyst was activated by 4.0 h of hydrogen flow (30 mL min^{-1}) at 450 ℃ and atmospheric pressure. For catalytic active tests, cyclohexane was introduced to the reactor system by bubbling H_2, through buffer bottle at 0 ℃ ice water bath. Gas hourly space velocity (GHSV) was 12000 mL g^{-1} h^{-1} (molar ratio of C_6H_{12} : H_2 = 1 : 25). The outlet stream of reactor was analyzed over an online gas chromatography (Agilent GC-7890A) equipped with flame ionization detector (FID) and HP-INNOWax capillary column.

3. Results and discussion

3.1 Textural properties

The chemical compositions and textural properties of the calcined Ni-Cu/SBA-15 catalysts and SBA-15 are presented in Table 1. The BET surface areas, total pore volumes and average pore diameters of the prepared samples are very close, due to the same metal loading and preparation method. Furthermore, the N_2 adsorption-desorption isotherms and BJH pore size distribution curves of all catalysts (Fig. S1) are also similar as well as that of blank SBA-15. Therefore, the ordered pore structure of catalysts is still kept well.

3.2 XRD analyzes

In Fig. 1a, the small-angle XRD patterns of SBA-15 and calcined catalysts show three peaks which ascribed to the (100), (110) and (200) planes of the ordered hexagonal mesoporous structure [32,33]. This also suggested the samples after calcination maintained the framework textural of SBA-15, confirmed the results obtained by nitrogen physisorption.

For the wide-angle XRD patterns of calcined catalysts, the distinct peak of metallic oxide (NiO or CuO) structure is observed in Fig. 1b. There are several diffraction peaks at 2θ = 35.8°, 39.0° and 48.9° attributed well to monoclinic CuO (JCPDS 48-1548), and at 2θ = 37.1°, 43.2° and 62.6° corresponded to NiO (JCPDS 78-0643). Fig. 1c shows the XRD patterns of spent catalysts. The spent 5Ni0Cu catalyst exhibits the major nickel metal

diffraction peaks at 2θ = 44.4° and 51.9° (JCPDS 04-0850), and 0Ni5Cu catalyst exhibits the major copper metal diffraction peaks at 2θ = 43.3° and 50.4° (JCPDS 04-0836). The diffraction peaks of other catalysts are located between the diffraction peaks of Ni and Cu. This result indicates Ni-Cu alloys formation in the bimetallic catalysts [31,36].

The average crystal sizes of fresh and spent catalysts have been calculated using Scherrer equation, and shown in Table 1. For the fresh catalysts, it seems that increasing Cu amount increases the crystallites size of metallic oxide. After reaction, the spent 4Ni1Cu and 3Ni2Cu exhibit smaller crystal size than that of 5Ni0Cu, and the particle sizes decrease from metallic oxide to metal, due to the Cu addition to preventing the sintering of the Ni-rich metallic particles [33,36]. It is obvious that the mean metal crystal size increases in the Cu-rich catalysts with the increase in Cu. The increase of this parameter could be related to that CuO and Cu have lower Tammann temperature than NiO and Ni [34]. The mean metal crystal sizes of all samples are larger than the average pore diameter of SBA-15. Nevertheless, the particles inside the pore could not become larger due to the space limitation of the ordered channels.

3.3 TEM study

The morphology and microstructure of Cu-rich samples after reaction were investigated by TEM analysis. The typical mesoporous structure with a narrow size distribution of SBA-15 is observed clearly in Fig. 2, confirming the results obtained by nitrogen physisorption and small-angle XRD. The metal species are nearly located inside the channels of SBA-15, or laid flat on the outside surface. This result indicates large amounts of highly dispersed metal particles distribute inside the pores of SBA-15. Furthermore, the distribution of Ni and Cu species was investigated by EDX elemental mapping in STEM mode (Fig. 2d and Fig. 2e). A good fusion performance of Ni and Cu is observed in the HAADF images of 3Ni2Cu and 2Ni3Cu catalysts, which indicates the formation of Ni-Cu alloys. This conclusion is in good agreement with the XRD results.

3.4 H_2-TPR analyzes

The TPR analysis of calcined samples was carried out, and performed in Fig. 3. For the pure NiO samples, one major reduction peak temperature at approximately 400 ℃ was observed, which is attributed to the reduction of Ni^{2+} into Ni^0 [37-40]. Whereas, 5Ni0Cu exhibits a lower temperature peak (326 ℃) and a large band (400-650 ℃). The lower temperature peak is attributed to the reduction of smaller NiO nanoparticles [41]. And the existence of large band and higher reduction temperature indicate the presence of NiO species strongly interacted with the support [42,43], or highly dispersed NiO species locating in the micropores of SBA-15 [41,44]. Similarly, 0Ni5Cu exhibits two peaks with maxima at 204 ℃ and 268 ℃ corresponding to two kinds of CuO particles. The first peak could be attributed to the highly dispersed and small CuO particles in the pores of SBA-15 and outside the pores. And the second peak could corresponded to CuO aggregated only on the external surface [45,46].

For the bimetallic samples, the low reduction temperature peak of NiO shifts to a lower temperature due to the addition of Cu, and becomes in line with the reduction peak of CuO with the increase in Cu. These results indicate a close contact between Ni and Cu or the formation of Ni-Cu alloy [33,35], in consistent with the analysis from XRD and TEM.

3.5 Surface analysis by XPS

XPS analysis was carried out to further investigate the chemical state of Ni and Cu on the surface of spent catalysts, and presented in Fig. 4 and Table 2. Typically, the main binding energy (BE) values of Ni in all the Ni-containing catalysts are 852.5-852.7 (Ni $2p_{3/2}$) and 870.1-870.3 eV (Ni $2p_{1/2}$), and their doublet separations are 17.4-17.6 eV, indicating the existence of only Ni^0 species [47]. This is in harmony with the XRD results. The Cu $2p_{3/2}$ spectra in all the Cu-containing catalysts shows a main broad peak in the range of 927 to 940 eV, which can be fitted into two peaks. The first one centered at 934.5 eV (Peak I) is assigned to CuO, and reveals that Cu species have been oxidized to Cu^{2+} during exposing the spent catalysts to air. Whereas, only diffraction peaks of metal Cu is observed from their XRD patterns (Fig. 2b) due to the presence of well-dispered Cu species on the external surface of SBA-15, as well as the internal surface. The peak centered at 932.1 eV (Peak II) is assigned to

metal Cu, deduced from their Cu $2p_{3/2}$ and doublet separations (19.4-19.6 eV) [48,49]. These may also imply the presence of two sizes of Cu particles, agreed with the TPR results.

For the bimetallic Ni-Cu catalysts, their Cu^0/Cu^{2+} atomic ratios increase along with Ni content. Moreover, the slight BE shifts of Ni^0 (0.1-0.2 eV) are observed, corrected well with the shift of Ni reduction peak. These results imply the presence of the strong interaction between Ni and Cu or the formation of Ni-Cu alloy [36,50,51]. Additionally, the surface Ni/Cu ratios are less than those of the bulk from preparation. This is mainly because of its lower Tammann temperature result in enriching easily on the surface at high temperature. Thus, Ni could play important role to stable and disperse metal Cu.

3.6 Catalytic activity for cyclohexane dehydrogenation

The catalytic activity of Ni-Cu/SBA-15 was evaluated for cyclohexane dehydrogenation, as presented in Fig. 5. The monometallic 5Ni0Cu exhibits high conversion but low selectivity. Notably, more than 50% of the byproduct CH_4 for 5Ni0Cu was detected at above 350 °C, as that reported previously on dehydrogenation reaction over Ni-based catalysts [8]. The 0Ni5Cu contained Cu-only produced only benzene and H_2 without any other byproducts, while its conversion is less than 20% and the lowest of all.

All bimetallic Ni-Cu/SBA-15 catalysts present better catalytic dehydrogenation performance than monometallic 5Ni0Cu and 0Ni5Cu. Remarkably, the addition of Cu to Ni-based catalysts improved drastically selectivity to benzene. In fact, this property for cyclohexane dehydrogenation over Ni-Cu catalysts has been reported [14,21,24] as written in the introduction. However, it is worth to highlight the good selectivity (> 90%) with high conversion (> 95%) at the range of 325 °C to 375 °C. In particular, 3Ni2Cu maintains an excellent selectivity (98.7%) with high conversion (99.4%) at 350 °C.

The dehydrogenation selectivity to benzene over Ni-Cu/SBA-15 catalyst increases as the Cu content increased, while cyclohexane conversion decreases. The same tendency for cyclohexane dehydrogenation on Ni-Cu catalysts has been also reported in our earlier literature [14]. More interesting, however, is that more excellent catalytic performance is observed on Ni-Cu/SBA-15, although higher metal content and smaller Ni-Cu bimetallic

nanoparticles exist in Ni-Cu/SiO_2 of the latter. This is mainly because of the formation of Ni-Cu alloy which is evidenced by XRD, H_2-TPR, TEM and XPS. With Cu incorporated into Ni-Cu alloy, Ni ensemble with low coordination number is shown to be a barrier to preventing methane formation [52]. Moreover, the conjunction between un-occupied d-band of Ni and full d-band of Cu weaken the activity of d-electron. Thus, the activity of the Ni-Cu alloy with an appropriate Ni/Cu ratio approaches to be "just right" for cyclohexane dehydrogenation.

The pore structure of SBA-15 was maintained well, which was confirmed by BET. Thus, amounts of metal active sites was supported and exposed. Moreover, the presence of monometallic Ni nanoparticles in the supported bimetallic catalysts is inevitable, especially with too small particle size. On the other side, large particle size for bimetallic Ni-Cu nanoparticles is effective to mix Ni and Cu, but not benefit the exposure of metal active sites. Results of this study indicate the existence of two sizes of bimetallic (or monometallic) particles in the Ni-Cu/SBA-15 catalysts, deduced from the analysis of H_2-TPR, BET and XRD. The small particles may play important role for catalytic active, due to its higher fraction of edge and corner metal atoms [52,53] and huge numbers.

3.7 Carbon deposition analyzes

The coke accumulated on the spent catalysts from the entire reaction test was analyzed by TG-DSC measurement (Fig. 6). Notably, an about 7% weight loss for 5Ni0Cu at the range of 400 ℃to 650 ℃is presented, and attributed to the combustion of coke [54,55]. And the weight loss deceases with the increase in Ni, as the same trend in catalytic dehydrogenation performance. This indicates the addition of Cu into Ni catalyst suppresses the formation of coke.

In fact, the monometallic Ni-based catalysts have been applied to research carbon nanotubes or carbon nanofiber by methane decomposition [56-58]. The carbon deposition for hydrocarbons dehydrogenation over Ni-containing catalysts is almost impossible to avoid. However, the improvement from crystal structure of metal Ni could repress the formation of coke. Thus, the Ni-Cu alloy keeps high resistance to carbon deposition.

3.8 In-situ DRIFT study

In order to identify the surface species of cyclohexane dehydrogenation over Ni-Cu/SBA-15 catalysts, an in-situ DRIFT study was performed. Firstly, the support SBA-15 was pretreated at 450 ℃ and in H_2 (5% in Ar) flow, and characterized (Fig. 7f) with DRIFT at 250 ℃ in the flow of C_6H_{12} + H_2 + Ar as the same process with catalysts. The difference spectra between in-situ DRIFT spectra of catalysts at different temperature and that of SBA-15 at 250 ℃ are shown in Fig. 7a-e. The in-situ DRIFT spectra of all samples can be found in Supplementary Material Fig. S2.

The peaks at 2319 and 2360 cm^{-1} on SBA-15 (Fig. 7f) ascribed to the absorption of CO_2 due to the difficult to be eliminated completely, and will not be discussed as follow [36]. The weak bands at 2863 and 2937 cm^{-1} correspond to the C-H symmetrical stretching and asymmetrical stretching of methylene [59-61]. These signals are ascribed to the absorption of cyclohexane on SBA-15.

For the in-situ DRIFT of Ni-Cu/SBA-15 in Fig. 9a-e, the peaks at 933 and 993 cm^{-1} are attributed to C-H out-of-plane bending of vinyl (=C-H) [60], indicating the existence of alkenes in the reactive intermediates. The weak band at 1570 cm^{-1} corresponds to C-C stretching within the ring. The bands at 1781 and 1934 cm^{-1} are weak combination and overtone bands appeared in the 1650-2000 cm^{-1} region [60]. These signals are attributed to the absorption of benzene. Furthermore, the change of their intensity with the increase in temperature is less than that of signals ascribed to the absorption of cyclohexane, indicating that the adsorption for benzene on catalyst is stronger. This could be the primary cause of coke deposition.

4. Conclusions

The bimetallic or monometallic particles are highly dispersed in the pores and on the external surface of SBA-15, and present two kinds of size due to the space limitation of the ordered channels. Nonetheless, the pore structure of SBA-15 is still kept well. For the dehydrogenation reaction of cyclohexane, the monometallic Ni catalyst presents highly catalytic activity, but low selectivity to benzene and serious carbon deposition. The addition of Cu into Ni drastically improves the selectivity, and prevents the coke formation. In

particular, 3Ni2Cu maintains an excellent selectivity (98.7%) with high conversion (99.4%) at 350 ℃ (GHSV = 12000 mL g^{-1} h^{-1}, molar ratio of C_6H_{12} : H_2 = 1 : 25). The in-situ DRIFT studies reveal the presence of vinyl species during the reaction. The strong absorption of benzene could lead to further dehydrogenation of benzene to coke.

Appendix A. Supplementary data

Supplementary data associated with this article could be found in the online version, at xxxx.

References

[1] F. Alhumaidan, D. Cresswell, A. Garforth, Hydrogen storage in liquid organic hydride: producing hydrogen catalytically from methylcyclohexane, Energy Fuels 25 (2011) 4217-4234.

[2] D.J. Durbin, C. Malardier-Jugroot, Review of hydrogen storage techniques for on board vehicle applications, Int. J. Hydrogen Energ. 38 (2013) 14598- 14617.

[3] A.U. Pradhan, A. Shukla, J.V. Pande, S. Karmarkar, R.B. Biniwale, A feasibility analysis of hydrogen delivery system using liquid organic hydrides, Int. J. Hydrogen Energ. 36 (2011) 680-688.

[4] Q.L. Zhu, Q. Xu, Liquid organic and inorganic chemical hydrides for high-capacity hydrogen storage, Energy Environ. Sci. 8 (2015) 478-512.

[5] C. Song, Fuel processing for low-temperature and high-temperature fuel cells challenges, and opportunities for sustainable development in the 21st century, Catal. Today 77 (2002) 17-49.

[6] Z. Qi, C. He, A. Kaufman, Effect of CO in the anode fuel on the performance of PEM fuel cell cathode, J. Powder Sources 111 (2002) 239-247.

[7] N. Jiang, K.S. Rao, M. Jin, S. Park, Effect of hydrogen spillover in decalin dehydrogenation over supported Pt catalysts, Appl. Catal. A 425-426 (2012) 62-67.

[8] Z. Kou, Z. Zhi, G. Xu, Y. An, C. He, Investigation of the performance and deactivation behavior of Raney-Ni catalyst in continuous dehydrogenation of cyclohexane under multiphase reaction conditions, Appl. Catal. A 467 (2013) 196-201.

[9] K. Akamatsu, Y. Ohta, T. Sugawara, T. Hattori, S. Nakao, Production of hydrogen by dehydrogenation of cyclohexane in high-pressure (1-8 atm) membrane reactors using amorphous silica membranes with controlled pore sizes, Ind. Eng. Chem. Res. 47 (2008) 9842-9847.

[10] D. Koutsonikolas, S. Kaldis, V.T. Zaspalis, G.P. Sakellaropoulos, Potential application of a microporous silica membrane reactor for cyclohexane dehydrogenation, Int. J. Hydrogen Energ. 37 (2012) 16302-16307.

[11] P.A. Antony, R.A. Sohony, R.B. Biniwale, An insight into spray pulsed reactor through mathematical modeling of catalytic dehydrogenation of cyclohexane, Int. J. Hydrogen Energ. 39 (2014) 6944-6952.

[12] H. Ping, G. Xu, S. Wu, System optimization of cyclohexane dehydrogenation under multiphase reaction conditions using the uniform design method, Int. J. Hydrogen Energ. 40 (2015) 15923-15932.

[13] E. Gianotti, M. Taillades-Jacquin, A. Reyes-Carmona, G. Taillades, J. Roziere, D.J. Jones, Hydrogen generation via catalytic partial dehydrogenation of gasoline and diesel fuels, Appl. Catal. B 185 (2016) 233-241.

[14] Z. Xia, H. Lu, H. Liu, Z. Zhang, Y. Chen. Cyclohexane dehydrogenation over Ni-Cu/SiO2 catalyst: Effect of copper addition, Catal. Commun. 90 (2017) 39-42.

[15] N. Kariya, A. Fukuoka, T. Utagawa, M. Sakuramoto, Y. Goto, M. Ichikawa, Efficient hydrogen production using cyclohexane and decalin by pulse-spray mode reactor with Pt catalysts, Appl. Catal. A 247 (2003) 247-259.

[16] B. Wang, G.F. Froment, D.W. Goodman, CO-free hydrogen production via dehydrogenation of a Jet A hydrocarbon mixture, J. Catal. 253 (2008) 239-243.

[17] G. Lee, Y. Jeong, B.G. Kim, J.S. Han, H. Jeong, H.B. Na, J.C. Jung, Hydrogen production by catalytic decalin dehydrogenation over carbon-supported platinum catalyst: Effect of catalyst preparation method, Catal. Commun. 67 (2015) 40-44.

[18] N. Boufaden, R. Akkari, B. Pawelec, J.L.G. Fierro, M.S. Zina, A. Ghorbel, Dehydrogenation of methylcyclohexane to toluene over partially reduced Mo–SiO_2 catalysts, Appl. Catal. A 502 (2015) 329-339.

[19] J. Li, Y. Chai, B. Liu, Y. Wu, X. Li, Z. Tang, Y. Liu, C. Liu, The catalytic performance of Ni_2P/Al_2O_3 catalyst in comparison with Ni/Al_2O_3 catalyst in dehydrogenation of cyclohexane, Appl. Catal. A 469 (2014) 434-441.

[20] A.H. Al-ShaikhAli, A. Jedidi, L. Cavallo, K. Takanabe, Non-precious bimetallic catalysts for selective dehydrogenation of an organic chemical hydride system, Chem. Commun. 51 (2015) 12931-12934.

[21] S.P. Patil, J.V. Pande, R.B. Biniwale, Non-noble NiCu/ACC bimetallic catalyst for dehydrogenation of liquid organic hydrides for hydrogen storage, Int. J. Hydrogen Energ. 38 (2013) 15233-15241.

[22] Z. Kou, S. Shen, K. Liu, G. Xu, Y. An, C. He, Kinetic analysis of dehydrogenation reaction of cyclohexane catalyzed by Raney-Ni under multiphase reaction conditions, Int. J. Hydrogen Energ. 38(2013) 11930-11936.

[23] J. Escobar, J.A.D.L. Reyes, T. Viveros, M.C. Barrera, Cyclohexane dehydrogenation over wet-impregnated Ni on Al_2O_3-TiO_2 Sol-Gel oxides, Ind. Eng. Chem. Res. 45 (2006) 5693-5700.

[24] J.H. Sinfelt, J.L. Carter, D.J.C. Yates, Catalytic hydrogenolysis and dehydrogenation over Copper-Nickel alloys, J. Catal. 24 (1972) 283-296.

[25] P.H. Desai, J.T. Richardson, Crystallite size effects in nickel catalysts: cyclohexane dehydrogenation and hydrogenolysis, J. Catal. 98 (1986) 392-400.

[26] I. Alstrup, M.T. Tavares, Kinetics of carbon formation from CH_4 + H_2 on silica-supported nickel and Ni-Cu catalysts, J. Catal. 139 (1993) 513-524.

[27] L.B. Avdeeva, O.V. Goncharova, D.I. Kochubey, V.I. Zaikovskii, L.M. Plyasova, B.N. Novgorodov, S.K. Shaikhutdinov, Coprecipitated Ni-alumina and Ni-Cu-alumina catalysts of methane decomposition and carbon deposition. II. Evolution of the catalysts in reaction, Appl. Catal. A 141 (1996) 117-129.

[28] I. Chen, F.L. Chen, Effect of alkali and alkaline-earth metals on the resistivity to coke formation and sintering of nickel-alumina catalysts, Ind. Eng. Chem. Res. 29 (1990) 534-539.

[29] M. Tasbihi, F. Feyzi, M.A. Amlashi, A.Z. Abdullah, A.R. Mohamed, Effect of the addition of potassium and lithium in Pt-Sn/Al_2O_3 catalysts for the dehydrogenation of isobutane, Fuel Process Technol. 88 (2007) 883-889.

[30] S. Takenaka, Y. Orita, H. Umebayashi, H. Matsune, M. Kishida, High resistance to carbon deposition of silica-coated Ni catalysts in propane stream reforming, Appl. Catal. A 351 (2008) 189-194.

[31] L-C. Chen, S.D. Lin, The ethanol steam reforming over Cu-Ni/SiO_2 catalysts: Effect of Cu/Ni ratio, Appl. Catal. B 106 (2011) 639-649.

[32] Q. Yao, Z-H. Lu, K. Yang, X. Chen, M. Zhu, Ruthenium nanoparticles confined in SBA-15 as highly efficient catalyst for hydrolytic dehydrogenation of ammonia borane and hydrazine borane, Sci. Rep. 5 (2015) 15186

[33] A. Ungureanu, B. Dragoi, A. Chirieac, S. Royer, D. Duprez, E. Dumitriu, Synthesis of highly thermostable copper-nickel nanoparticles confined in the channels of ordered mesoporous SBA-15 silica, J. Mater. Chem. 21 (2011) 12529-12541.

[34] A. Ungureanu, B. Dragoi, A. Chirieac, C. Ciotonea, S. Royer, D. Duprez, A.S. Mamede, E. Dumitriu, Composition-dependent morphostructural properties of Ni-Cu oxide nanoparticles confined within the channels of ordered mesoporous SBA-15 silica, ACS Appl. Interfaces 5 (2013) 3010-3025.

[35] L-C. Chen, H. Cheng, C-W. Chiang, S.D. Lin, Sustainable hydrogen production by ethanol steam reforming using a partially reduced Copper–Nickel oxide catalyst, ChemSusChem 8 (2015) 1787-1793.

[36] E.T. Saw, U. Oemar, X.R. Tan, Y. Du, A. Borgna, K. Hidajat, S. Kawi, Bimetallic Ni–Cu catalyst supported on CeO2 for high-temperature water–gas shift reaction: Methane suppression via enhanced CO adsorption, J. Catal. 314 (2014) 32-46.

[37] Y. Kobayashi, J. Horiguchi, S. Kobayashi, Y. Yamazaki, K. Omata, D. Nagao, M. Konno, M. Yamada, Effect of NiO content in mesoporous NiO–Al_2O_3 catalysts for high pressure partial oxidation of methane to syngas, Appl. Catal. A 395 (2011) 129-137.

[38] Y.H. Wang, H.M. Liu, B.Q. Xu, Durable Ni/MgO catalysts for CO_2 reforming of methane: Activity and metal–support interaction, J. Mol. Catal. A 299 (2009) 44-52.

[39] L. Bednarczuk, P.R. Piscina, H. Narcis, H_2-production from CO_2-assisted ethanol steam reforming: The regeneration of Ni-based catalysts, Int. J. Hydrogen Energ. 40 (2015) 5256-5263.

[40] W.S. Dong, H.S. Roh, K.W. Jun, S.E. Park, Y.S. Oh, Methane reforming over Ni/Ce-ZrO_2 catalysts: effect of nickel content, Appl. Catal. A 226 (2002) 63-72.

[41] Y. Park, T. Kang, J. Lee, P. Kim, H. Kim, J. Yi, Single-step preparation of Ni catalysts supported on mesoporous silicas (SBA-15 and SBA-16) and the effect of pore structure on the selective hydrodechlorination of 1,1,2-trichloroethane to VCM, Catal. Today 97 (2004) 195-203.

[42] M. Tao, X. Meng, Z. Xin, Z. Bian, Y. Lu, J. Gu, Synthesis and characterization of well dispersed nickel-incorporated SBA-15 and its high activity in syngas methanation reaction, Appl. Catal. A 516 (2016) 127-134.

[43] E. Byambajav, Y. Ohtsuka, Hydrocracking of asphaltene with metal catalysts supported on SBA-15, Appl. Catal. A 252 (2003) 193-204.

[44] A.G. Gil, Z. Wu, D. Chadwick, K. Li, Ni/SBA-15 Catalysts for combined steam methane reforming and water gas shift—prepared for use in catalytic membrane reactors, Appl. Catal. A 506 (2015) 188-196.

[45] R. Lin, M.F. Luo, Y.J. Zhong, Z.L.Yan, G.Y. Liu, W.P. Liu, Comparative study of $CuO/Ce_{0.7}Sn_{0.3}O_2$, CuO/CeO_2 and CuO/SnO_2 catalysts for low-temperature CO oxidation, Appl. Catal. A 255 (2003) 331-336.

[46] C.H. Tu, A.Q. Wang, M.Y. Zheng, X.D. Wang, T. Zhang, Factors influencing the catalytic activity of SBA-15-supported copper nanoparticles in CO oxidation, Appl. Catal. A 297 (2006) 40-47.

[47] F.U. Hillebrecht, J.C. Fuggle, P.A. Bennett, Z. Zolnierek, Electronic structure of Ni and Pd alloys. II. X-ray photoelectron core-level spectra, Phys. Rev. B 27 (1983) 2179-2193.

[48] B.R. Strohmeier, D.E. Leyden, R.S. Field, D.M. Hercules, Surface spectroscopic characterization of $Cu/A1_2O_3$ catalysts, J. Catal. 94 (1985) 514-530.

[49] J.C. Fuggle, E. Kallne, L.M. Watson, D.J. Fabian, Electronic structure of aluminum and aluminum-noble-metal alloys studied by soft-x-ray and x-ray photoelectron spectroscopies, Phys. Rev. B 16 (1977) 750-761.

[50] P.A. Bennett, J.C. Fuggle, F.U. Hillebrecht, Electronic structure of Ni and Pd alloys. III. Correlation effects in the Auger spectra of Ni alloys, Phys. Rev. B 27(1983) 2194-2209.

[51] K.R. Harikumar, S. Ghosh, C.N.R. Rao, X-ray photoelectron spectroscopic investigations of Cu-Ni, Au-Ag, Ni-Pd, and Cu-Pd bimetallic clusters, J. Phys. Chem. A 101 (1997) 536-540.

[52] L. Gan, R. Tian, X. Yang, H. Lu, Y. Zhao, Catalytic reactivity of CuNi alloys toward H_2O and CO dissociation for an efficient water gas shift: A DFT study, J. Phys. Chem. C 116 (2012) 745-752.

[53] A.L.M. Silva, J.P. Breejen, L.V. Mattos, J.H. Bitter, K.P. Jong, F.B. Noronha, Cobalt particle size effects on catalytic performance for ethanol steam reforming – Smaller is better, J. Catal. 318 (2014) 67-74.

[54] A. Carrero, J.A. Calles, A.J. Vizcaino, Hydrogen production by ethanol steam reforming over Cu-Ni/SBA-15 supported catalysts prepared by direct synthesis and impregnation, Appl. Catal. A 327 (2007) 82-94.

[55] C. Ding, J. Wang, G. Ai, S. Liu, P. Liu, K. Zhang, Y. Han, X. Ma, Partial oxidation of methane over silica supported Ni nanoparticles with size control by alkanol solvent, Fuel 175 (2016) 1-12.

[56] A.A. El Mel, E. Gautron, B. Angleraud, A. Granier, P.Y. Tessier, Synthesis of nickel-filled carbon nanotubes at 350 °C, Carbon 49 (2011) 4595-4607.

[57] S. Takenaka, S. Kobayashi, H. Ogihara, K. Otsuka, Ni/SiO_2 catalyst effective for methane decomposition into hydrogen and carbon nanofiber, J. Catal. 217 (2003) 79-87.

[58] S. Takenaka, H. Ogihara, K. Otsuka, Structural change of Ni species in Ni/SiO_2 catalyst during decomposition of methane, J. Catal. 208 (2002) 54-63.

[59] Y. Yu, H. He, Q. Feng, H. Gao, X. Yang, Mechanism of the selective catalytic reduction of NOx by C_2H_5OH over Ag/Al_2O_3, Appl. Catal. B 49 (2004) 159-171.

[60] R.M. Silverstein, F.X. Webster, D.J. Kiemle, D.L. Bryce, Spectrometric Identification of Organic Compounds, 7th ed., In: Infrared spectrometry, John Wiley & Sons Inc, New York, 2005, pp. 72-126.

[61] J. Wood, M.J. Alldrick, J.M. Winterbottom, E.H. Stitt, S. Bailey, Diffuse reflectance infrared Fourier transform spectroscopy (DRIFTS) study of ethyne hydrogenation on Pd/Al_2O_3, Catal. Today 128 (2007) 52-62.

List of figure captions

Fig. 1. XRD patterns of samples. (a) Small-angle and (b) wide-angle XRD patterns for calcined catalysts. (c) Wide-angle XRD patterns for spent catalysts.

Fig. 2. TEM images of the spent catalysts. (a) 3Ni2Cu, (b) 2Ni3Cu, (c) 0Ni5Cu, (d) HAADF-STEM images of 3Ni2Cu and (e) HAADF-STEM images of 2Ni3Cu.

Fig. 3. TPR patterns of calcined catalysts.

Fig. 4. XPS spectra of (a) Ni 2p and (b) Cu 2p for spent catalysts.

Fig. 5. Catalytic properties of Ni-Cu/SBA-15 in cyclohexane dehydrogenation. Reaction condition: 150mg catalyst, total 101 kPa, C_6H_{12} : H_2 = 1 : 25, GHSV = 12000 h^{-1}.

Fig. 6. TG and DSC patterns of spent catalysts.

Fig. 7. In-situ DRIFT study over Ni-Cu/SBA-15 catalysts in the flow of C_6H_{12} + H_2 + Ar. (a) 5Ni0Cu, (b) 4Ni1Cu, (c) 3Ni2Cu, (d) 2Ni3Cu, (e) 0Ni5Cu and (f) SBA-15.

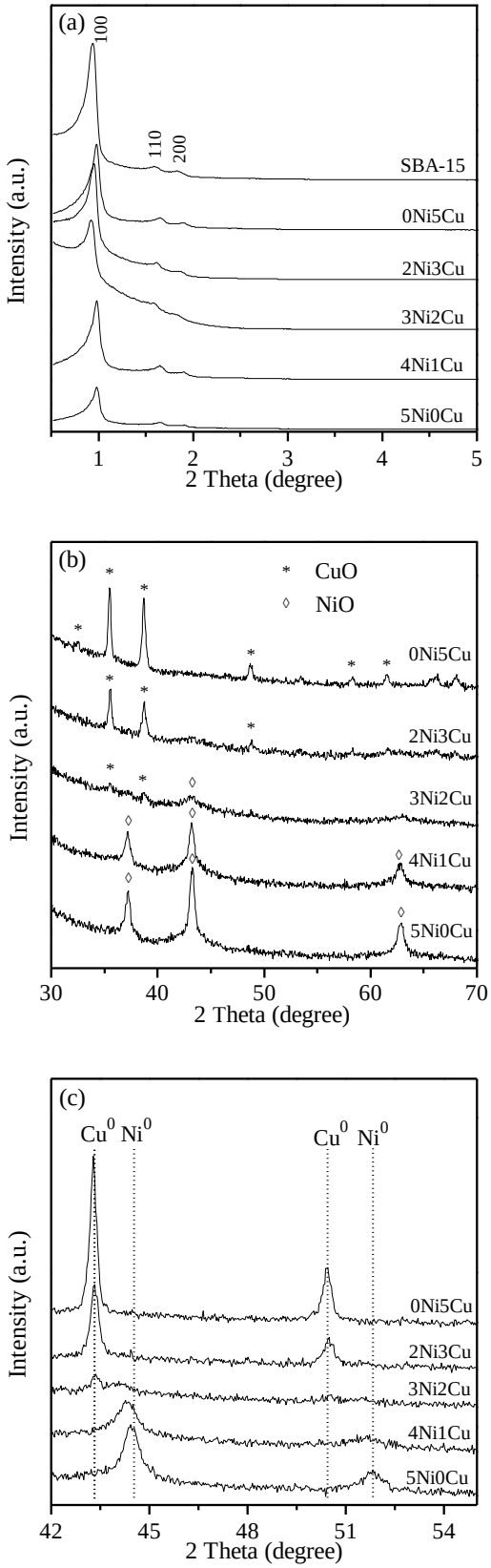

Fig. 1

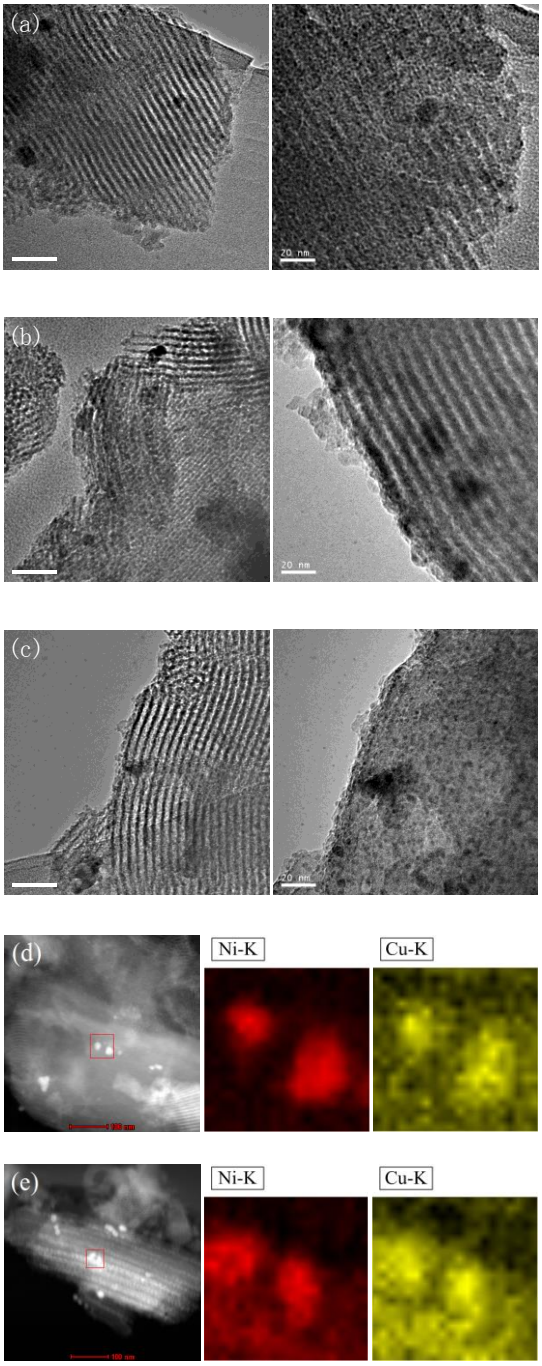

Fig. 2

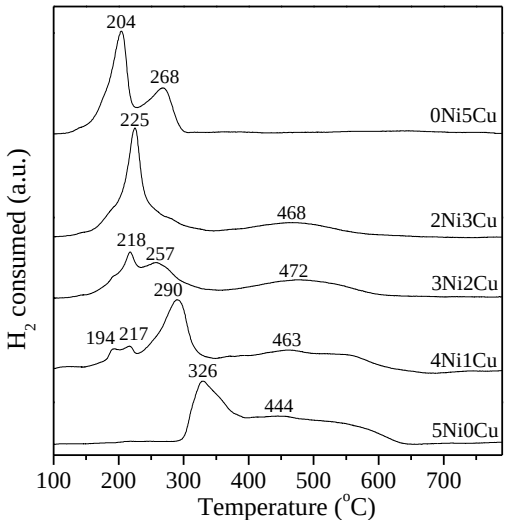

Fig. 3

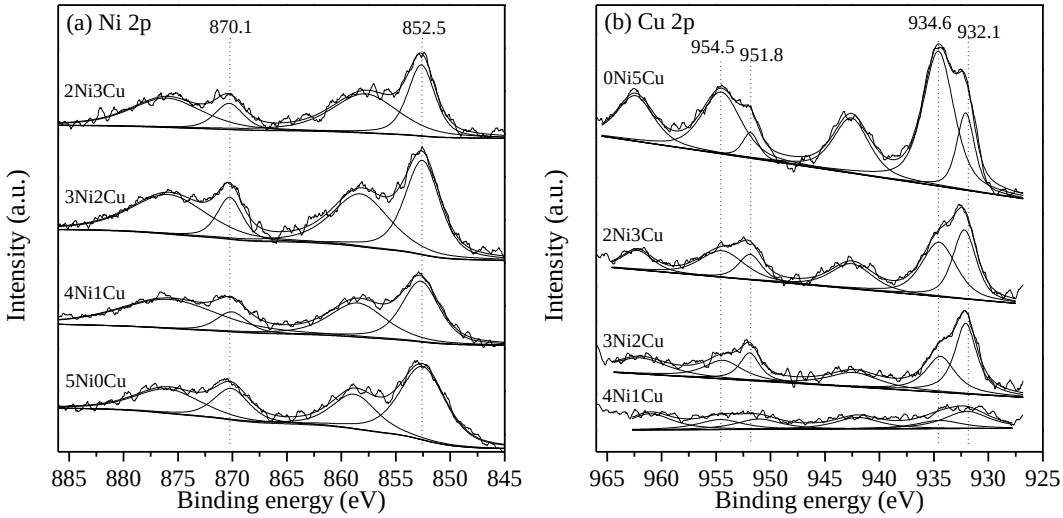

Fig. 4

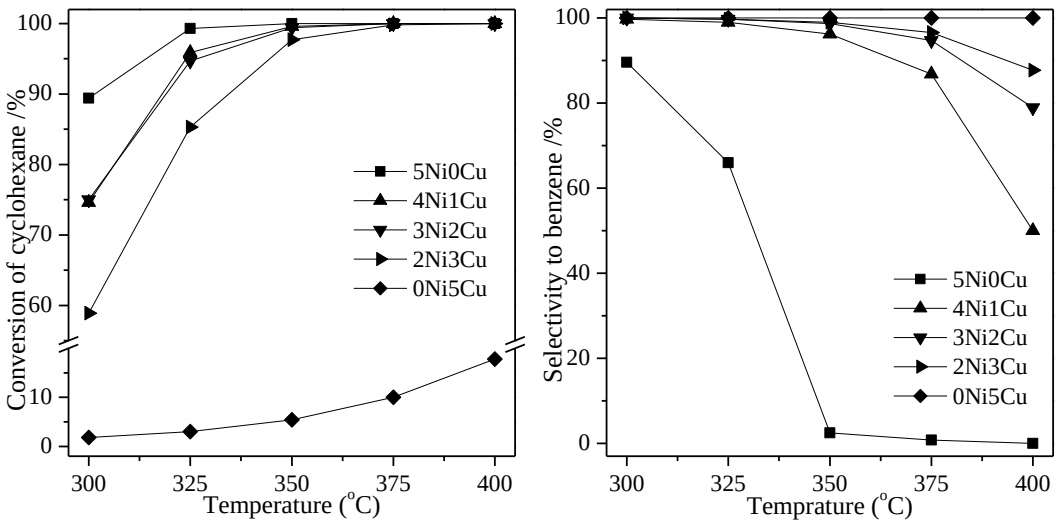

Fig. 5

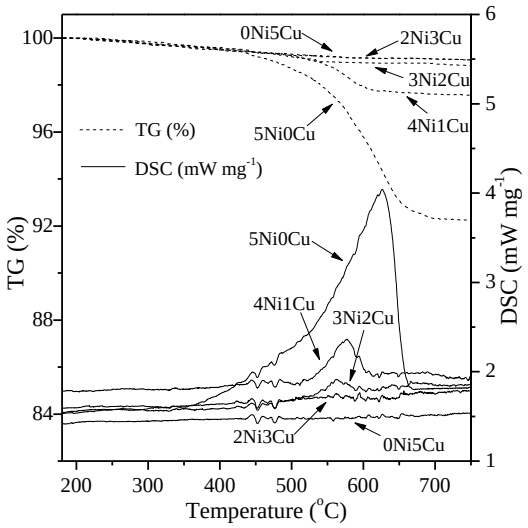

Fig. 6

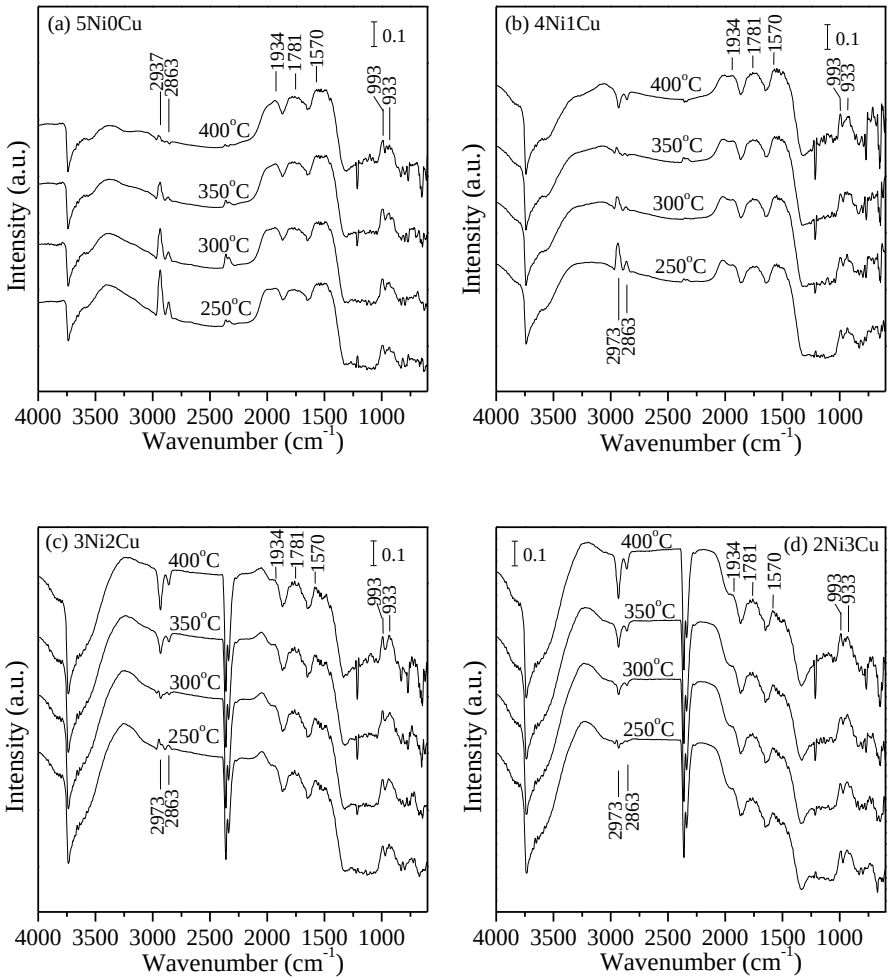

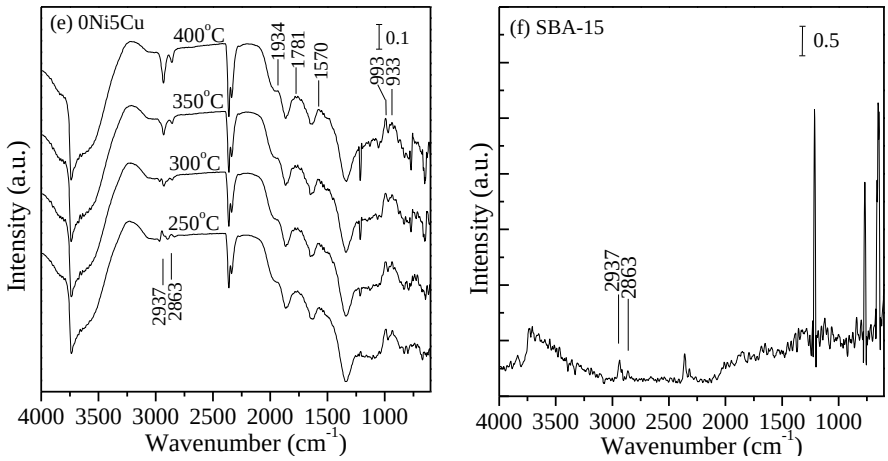

Fig. 7

Table captions

Table 1

The physicochemical properties of calcined Ni-Cu/SBA-15 catalysts.

Sample /SBA-15	Ni [a] (wt.%)	Cu [a] (wt.%)	S_{BET} (m^2 g^{-1})	V_{pore} (cm^3 g^{-1})	D_{pore} (nm)	Average crystal size [b] (nm)	
						Metallic oxide	Metal
5Ni0Cu	8.12	0	504.4	0.76	6.00	18.6 (NiO)	19.5 (Ni)
4Ni1Cu	6.48	1.75	509.3	0.76	6.04	19.5 (NiO)	16.7 (Ni)
3Ni2Cu	4.86	3.49	505.7	0.75	5.92	19.6 (CuO)	18.3 (Cu)
2Ni3Cu	3.23	5.23	501.9	0.75	5.99	26.7 (CuO)	34.2 (Cu)
0Ni5Cu	0	8.70	500.8	0.75	5.96	31.5 (CuO)	38.1 (Cu)
SBA-15	0	0	685.4	0.95	5.54	0	0

[a] Metal / (Metal + SiO_2) as determined from the preparation of catalyst.

[b] Calculated using Scherrer equation from the XRD patterns of fresh (Metallic oxide) and spent (Metal) catalysts.

Table 2

XPS analysis of spent Ni-Cu/SBA-15 catalysts.

Catalyst	Ni $2p_{3/2}$ [a]	Ni $2p_{1/2}$ [a]	Cu $2p_{3/2}$ [a, b]		Cu $2p_{1/2}$ [a]		Ni/Cu [c]
			Peak I	Peak II	Peak III	Peak IV	
5Ni0Cu	852.5	870.1	-			-	-
4Ni1Cu	852.7	870.1	934.5 (32)	932.0 (68)	954.6	951.4	3.16
3Ni2Cu	852.6	870.2	934.4 (41)	932.1 (59)	954.4	951.8	1.89
2Ni3Cu	852.7	870.3	934.5 (53)	932.2 (47)	954.5	951.8	0.94
0Ni5Cu	-	-	934.6 (75)	932.1 (25)	954.5	951.8	0

[a] Binding energy (eV).

[b] Numbers in parentheses represent the relative contribution calculated using the peak area.

[c] Surface atomic ratios.